PERGAMON

Journal of Structural Geology 21 (1999) 1535–1551

JOURNAL OF STRUCTURAL GEOLOGY

www.elsevier.nl/locate/jstrugeo

Ductile shear zones as counterflow boundaries in pseudoplastic fluids

Christopher J. Talbot

Hans Ramberg Tectonic Laboratory, Department of Earth Sciences, Uppsala University, Norbyvägen 16, S-752 36 Uppsala, Sweden

Received 16 September 1998; accepted 30 May 1999

Abstract

Ductile shear zones with different styles are attributed to rocks having deformed as pseudoplastic power law fluids with different exponents $n > 1$ of the stress sensitivity of the strain rate. Profiles of velocity and accumulated displacements recorded by passive markers in pseudoplastic fluids flowing steadily and continuously along no-slip boundaries have robust geometries distinctive of the n-value. What have previously been considered as single shear zones are forward modelled as pairs of back-to-back boundary shears coupled across individual counterflow boundaries.

Displacement gradients in natural shear zones are shown to fit theoretical displacement curves for steady flows of pseudoplastic fluids along no-slip boundaries in a variety of rock types of different age, environment and scale. General fits of these curves indicate that strain was homogeneous along natural counterflow boundaries, so that specific values or ranges of n-value can be assigned to the rocks when they sheared whatever deformations and deformation mechanisms were involved. Fits that are only local indicate inhomogeneous strains along natural boundary shears and require more detailed analysis.

1. Introduction

The distortion within ductile shear zones of markers, old or new, record shear strains that are zero along sub-parallel margins and increase inward to a near-central surface from which relative displacement increases outward to maxima along the margins. Shear zones along lithological contacts are characteristically asymmetric but those that cross otherwise uniform rock masses are closer to symmetric.

The only constant volume strain that can occur in straight parallel-sided zones between bodies of unstrained rocks is simple shear (Ramsay and Graham, 1970; Simpson and De Paor, 1993) which should also be continuous (Lister and Williams, 1979) and homogeneous (Jiang and White, 1995). Zones of steady and continuous simple shear with constant volume will therefore be considered before some of the potential complications.

The localisation of shear into particular zones in rocks has previously been attributed to local softening by processes that are geometric (Harris and Cobbold, 1984), chemical (Beach, 1985), and structural, mechanical or thermal (Mitra, 1978; Poirier, 1980; Kameyama et al., 1997) in any combination. However, until now, there has been no simple paradigm accounting for the spontaneous localisation of ductile shear into narrow zones.

This work presents a new conceptual model for shear zones and how they develop. It develops one of the simplest of previous theoretical models, that shear zones are merely ductile faults in power law fluids that strain rate soften (Poirier, 1980). Velocity and displacement gradients of power law fluids flowing beside a particular type of no-slip boundary are used to forward model shear zones that look realistic. Natural shear zones in the field and literature are then shown to display essentially similar displacement gradients. In effect, the large range of geometries anticipated along natural shear zones (Jiang and White, 1995) are limited to a particular set of curves which measure the stress

E-mail address: Christopher.Talbot@geo.uu.se (C.J. Talbot)

0191-8141/99/$ - see front matter
PII: S0191-8141(99)00113-3

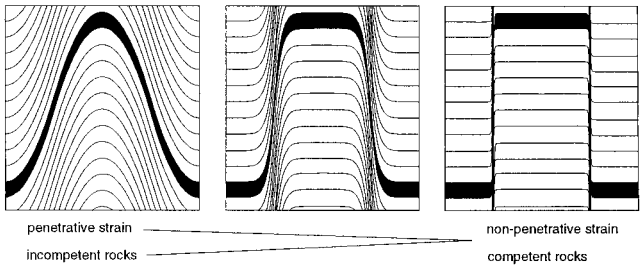

Fig. 1. The shear spectrum.

sensitivity of the strain rates of adjoining rock masses when they sheared.

2. The shear spectrum

Whatever their scales, ductile shear zones lie in a geometric spectrum with wide zones of gentle shear inconspicuous along the limbs of flow folds at one end and, at the other end, zones of intense shear so narrow that they resemble faults (Fig. 1). However, faults are discontinuities, and the essence of ductile shear zones is the continuity of shear gradients across them. This geometric spectrum is generally considered to relate to a mechanical spectrum expressed in terms of either penetration of strain or competence, both qualitative concepts for which a single quantitative alternative will be suggested here (Fig. 1).

To model and interpret shear zones we need a rheology that specifies shear localising to degrees related to specific variables. Here such a quantitative spectrum is based on power law fluids.

3. Power law fluids

Power law fluids are those where the shear stress, τ, or the stress difference, σ $(=\sigma_1-\sigma_3)$ and the corresponding steady rates of shear, $\dot{\gamma}$, or longitudinal strain, $\dot{\varepsilon}$ are related by

$$\tau = A\dot{\gamma}\,1/n \tag{1a}$$

$$\sigma = A\dot{\varepsilon}^{1/n} \tag{1b}$$

or

$$\dot{\varepsilon} = A\sigma^{n} \tag{1c}$$

(Eq. 1a, Wilkinson, 1960; Eq. 1b and c, Means, 1990).

The constants, A, in Eq. 1(a–c) are not necessarily equal but are general functions of pressure, temperature and material parameters (see later); the $\dot{}$ indicates the time derivative. The exponent n is the stress sensitivity of the strain rate (Harris, 1977; Means, 1990), while its reciprocal, $1/n$, is the strain rate sensitivity of the flow stress (Means, 1990).

Newtonian fluids deform with $n=1$ so that strain rates have a linear relationship with stress. Where $n\neq 1$, the n-value measures the degree of non-Newtonian behaviour; the greater its departure from unity, the more non-linear are the properties of the fluid. Fluids for which n is below unity, dilatant fluids, are said to strain rate harden. However, the focus here will be on pseudoplastic fluids, for which the n-value is above unity and which conventionally strain rate soften. The softening refers to a decrease in apparent viscosity, the current ratio of stress to strain rate, not the resistance to shearing (Means, personal communication, 1999). Fluid mechanics attribute pseudoplasticity to increasing rates of shear enhancing the preferred orientations of asymmetric particles (Wilkinson, 1960) with shapes that may also increase in symmetry. The n-value is taken here as a simple measure of the localisation of shear strain in rocks.

Until the mid 1970s, theoretical geoscientists generally considered ductile rocks as Newtonian fluids that deform by diffusion. However, by then laboratory results with rocks deforming by a combination of dislocation and diffusion mechanisms until creep was steady under constant stress were usually fit by power laws with significant non-linearity, e.g. $n=3$–10 (e.g. Heard, 1968). Laboratory creep rates are over five orders of magnitude faster than is likely in nature. Nevertheless, increasing use of power law rheologies for ductile rocks since Fletcher (1974) has improved quantitative agreement between theory and natural deformation structures (e.g. Smith, 1977; Turcotte and Schubert, 1982; Tackley, 1998). A general decrease in n with decreasing strain rate is likely on both mathematical and physical grounds (Smith, 1977). Shear will be shown to concentrate in zones in association with a particular type of boundary.

3.1. Velocity and displacement gradients beside a no-slip boundary

Deformation boundaries can allow free-slip, stick-slip or no-slip; they can also be rigid or flexible, etc. Just as shear in brittle rock masses occurs along discrete new or old free-slip or stick-slip boundaries, shears in ductile rocks develop along new or old no-slip boundaries. A start is made by focusing on the steady flow of power law fluids between two planar no-slip rigid boundaries and then skewing this situation inside out.

Consider the flow of a power law fluid driven by pressure difference ΔP along a channel of length L and width, w, between *two* stationary rigid walls (Turcotte and Schubert, 1982). The shear stress in the fluid satisfies:

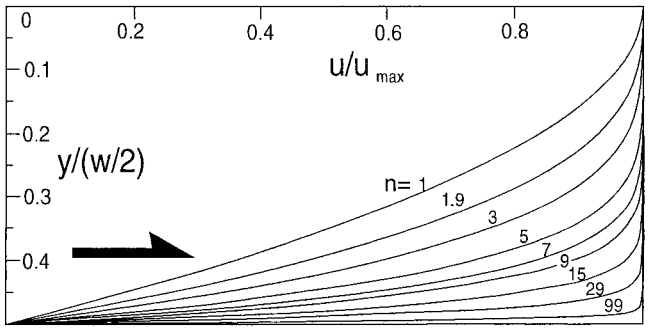

Fig. 2. Non-dimensional profiles of velocity, u/u_{max}, plotted against distance, $y/(w/2)$ from a no-slip boundary for steady flow of pseudoplastic fluids. Strain rate sensitivities are given by n-values on curves (from Eq. 5).

$$d\tau/dy = -\Delta P/L \quad (2)$$

(Eq. 2, Turcotte and Schubert, 1982, p. 316). For a power law fluid the shear stress and velocity gradient, or strain rate, are related by

$$du/dy = C\tau^n \quad (3)$$

(Eq. 3, Turcotte and Schubert, 1982, p. 316) where C is a constant and n a positive integer. Solving Eq. (3) for τ and substituting into Eq. (2) and then integrating for the above symmetry conditions and then integrating for no-slip boundary conditions (Turcotte and Schubert, 1982, p. 318) results in

$$u = C/(n+1)\{\Delta P/L\}^n\{(w/2)^{n+1} - y^{1+n}\} \quad (4)$$

(Eq. 4, Turcotte and Schubert, 1982, p. 318). We can focus on the velocity beside a *single* no-slip boundary by normalising the velocity, u by its maximum, u_{max} which yields

$$u/u_{max} = 1 - (2y/w)^{n+1} \quad (5)$$

(Eq. 5, Bertram Schott, personal communication, 1999). Here y is the co-ordinate perpendicular to the boundary. The effective viscosity of the power law fluid is proportional to τ^{1-n} (Turcotte and Schubert, 1982, p. 318).

Equation (5) with u/u_{max} normalised to twice $y/(w/2)$ (Fig. 2) allows comparison between velocity profiles in power law fluids with different n flowing steadily beside a single planar no-slip boundary.

The flow of a Newtonian fluid ($n = 1$) driven by a pressure difference along a no-slip boundary is penetrative but not uniform and its parabolic velocity profile simulates part of a flow fold (Fig. 1). The velocity and displacement profiles of pseudoplastic fluids ($n > 1$) depend upon their n-value (Fig. 2). This is so even though the shear stresses for all n-values share the same linear gradient. As the n-value of the fluid increases, the velocity profile develops a shoulder with a radius of curvature that decreases as it migrates toward the no-slip boundary (Fig. 2). Further, the velocity gradients steepen and increasingly localise to the no-slip boundary so that the boundary effect reaches smaller distances into what is increasingly 'plug flow'. As n exceeds ≈ 29, boundary shears resemble faults. Velocity profiles for pseudoplastic fluids (Fig. 2) are also finite displacement profiles of appropriate markers at particular times, such as after flow has ceased.

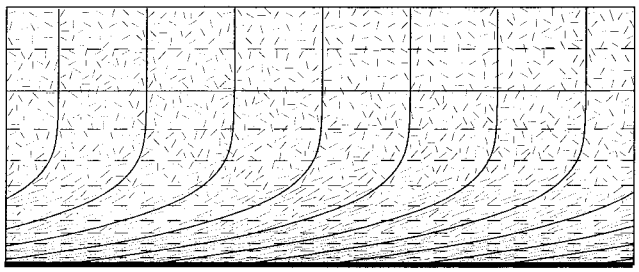

Fig. 3. Distortion of markers in a pseudoplastic fluid ($n = 3$) due to the velocity gradient imparted by steady flow being retarded along a rigid no-slip boundary (thickened base) up to the nominal margin (thin continuous line) of a boundary shear.

Each of the velocity or displacement profiles in Fig. 2 remains distinctive of the n-value whatever the maximum velocity, displacement or width. This is because the effective viscosity in pseudoplastic fluids is lowest where the shear stress is highest, along the no-slip boundary, and highest where the shear stress is lowest, beyond the retarding effect of the no-slip boundary.

3.2. Markers in boundary shears

Fig. 3 shows three types of passive markers distorted in a *boundary shear*. Distortion induced by traction along the boundary shear's rigid basal no-slip boundary (thickened) penetrates the fluid as far as its upper margin (thin continuous line) beyond which the markers retain their initial configurations. Each in their own way show that shear strains increase to a maximum along the no-slip boundary while displacements increase away from it to a maximum maintained throughout the fluid mass beyond the margin.

Continuous thin lines initially perpendicular to the shear (Fig. 3) map velocity gradients and accumulated displacement gradients across the boundary shear in a pseudoplastic fluid flowing with $n = 3$ after an arbitrary time (as repetitions of the $n = 3$ curve from Fig. 2). A nominally random (isotropic) fabric has developed a new, shear-induced fabric within the boundary shear. Each component of the fabric rotates passively so that the preferred fabric orientation parallels the long axis of the strain ellipse and intensifies as it rotates toward the no-slip boundary. Particle movement paths (dashed) map stream lines that parallel the direction of simple shear with spacings that narrow

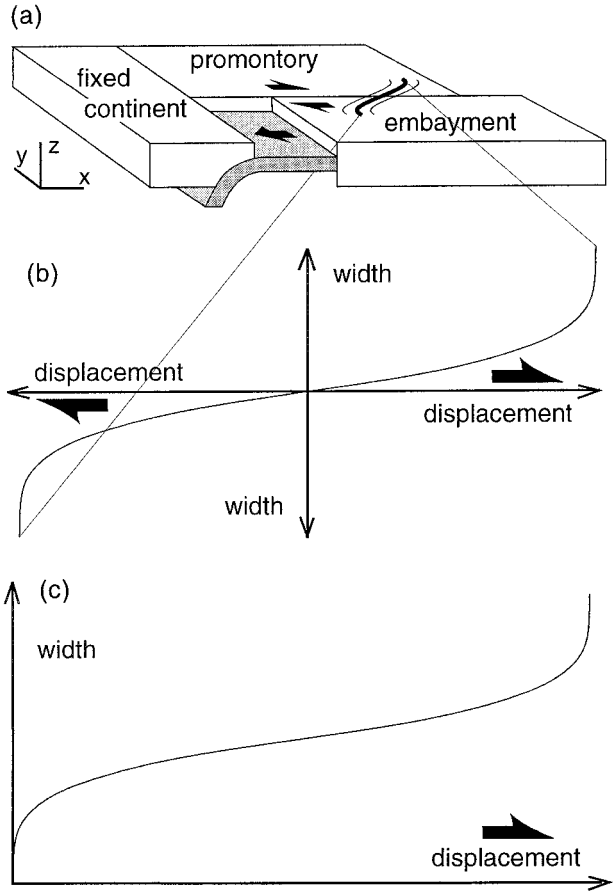

Fig. 4. Reference frames for deformation zones. (a) Frame fixed in non-subducting continent with an embayment in another continent shearing past a promontory on a subducting plate converging in the same direction at different rates. (b) Frame fixed to the mutual no-slip boundary between two boundary shears. (c) Frame fixed on one margin. Frames (b) and (c) are practical but do not show the boundary conditions responsible for shear zones in initially uniform rocks.

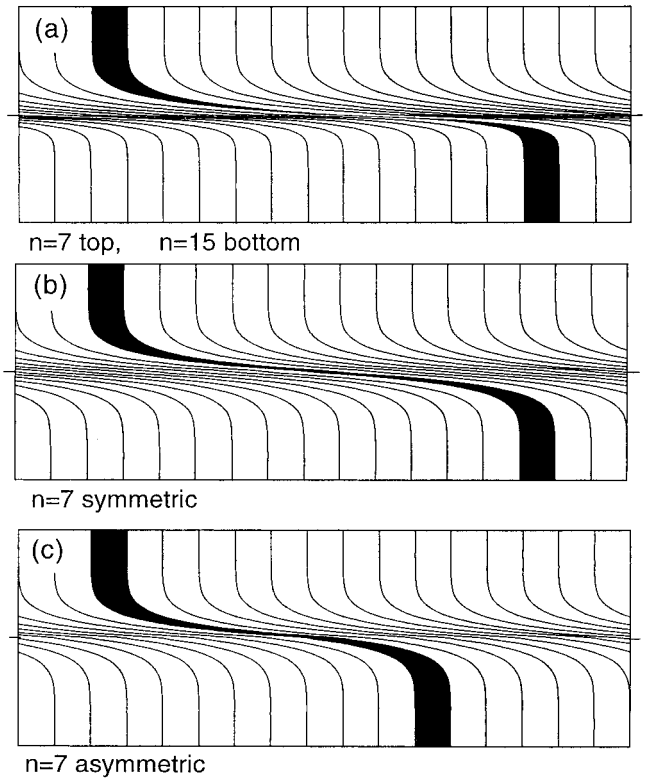

Fig. 5. (a) Counterflow boundary shears in pseudoplastics of different *n*-value are asymmetric in both width and displacement. (b) Counterflow shears in masses of identical pseudoplastics that travelled in the same direction at rates that differed by a factor of 2 are symmetric. (c) Boundary shears in identical pseudoplastics that travelled in the same direction at rates differing by any factor other than 2 are asymmetric in displacement but not necessarily width.

toward the no-slip boundary. Because the stream lines are parallel, flow in the boundary shear has been homogeneous and steady. Had passive marker lines initially paralleled the no-slip boundary, they would have remained straight and retained their initial lengths and spacings. Shear bands (not shown) could have developed in various orientations (Jiang and White, 1995).

Most geologists probably consider Fig. 3 as showing only half a shear zone but here we follow fluid mechanics and treat it as a single boundary shear.

3.3. Kinematics and reference frames

It is not necessary for the material beneath the no-slip boundaries in Fig. 3 to be rigid. Visualise another body of fluid with similar markers beneath the no-slip boundary in Fig. 3, one that is identical to that above and flowing in the same direction at a different rate. What would happen to passive markers on either side of the single mutual no-slip boundary?

An analogous situation is a vertical shear zone developing in a continent in which an embayment (behind still-subducting ocean floor) is shearing past an already sutured promontory (Fig. 4a). The shear zone records the relative difference between the rates of motion of the promontory and embayment. Both the promontory and embayment are travelling in the same direction in a Lagrangian reference frame fixed to the continent on the non-subducting plate (Fig. 4a). However, *relative to each other*, and in an Euler reference frame fixed to the central plane of the zone, they are flowing in opposite directions (Fig. 4b). Ramsay and Graham (1970) began by fixing their reference frame to the central plane (Fig. 4b) but, without explanation, ended using the reference frame shown in Fig. 4(c). Most subsequent workers have used this frame (Fig. 4c) fixed in one of two passive (Mitra, 1978) or unstrained 'walls' (Ramsay, 1980). The adjectives passive or unstrained are entirely appropriate for bodies of fluids flowing at different rates beyond their mutual boundary shears but, applied to walls, tend to lead to

the unnecessary concept that the two fluids are rigid in ways other than mathematical.

The Eulerian reference frames in Fig. 4(b) and (c) are practical for field geologists but neither relate displacements or shear strains to any external boundaries that may have retarded one fluid mass more than the other (as is obvious in Fig. 4a).

The frame in Fig. 4(c) illustrates that displacements on both sides of a shear zone (and therefore the velocities during deformation) may share the same direction and sense of shear. Its general use accounts for why geologists habitually refer to structures like those in each box of Fig. 5 as *single* left-handed ductile shear zones.

3.4. Counterflow boundaries

Considering shear zones as single structures misses the fact that the bodies on either side have moved in opposing relative directions along a particular plane. No relative displacement has occurred at that plane and the shear strains are largest in both boundary shears at that same plane which can therefore be treated as a mutual no-slip boundary. The reference frame in Fig. 4(b) is therefore used here to illustrate that what have previously been thought of as an individual shear zone might be more usefully considered as pairs of boundary shears back-to-back across common no-slip boundaries. Treating 'individual shear zones' as coupled pairs of boundary shears allows a direct inverse linkage between displacements and shear strains. Coupled boundary shears can differ in symmetry (width and/or maximum displacement) so the shared no-slip boundary is the central plane only between symmetrical boundary shears.

A no-slip boundary between two fluid masses flowing in relatively opposed directions is a special category of boundary, referred to here as a *counterflow boundary*. Shear strains on either side of the counterflow boundary concentrate in each of the boundary shears to degrees that depend on the n-values of the counterflowing fluids.

Gradients in flow velocity localise in space or time along two types of counterflow boundaries: those along lithological boundaries and those that develop across initially uniform rocks.

Because the strain rates on either side of lithological boundaries are intrinsically different, the maximum displacement and/or widths of the two coupled boundary shears are necessarily asymmetric (Fig. 5a). It has been shown that shears along such strain-active boundaries can remain neither steady (Lister and Williams, 1979) nor simple (Jiang, 1994). Such complications can lead to the basic shear instability that generates lobes in the rock with higher viscosity and cusps in the rock with lower viscosity (Ramsay, 1967). The sense of shear reverses at every cusp and lobe. If boundary shears along two lithological boundaries are sufficiently wide to interact, their mutual interference can result in either buckles (or flow boudins) along shortened (or extended) single layers of relatively high effective viscosity. Alternatively, interference can result in fold mullions (or inverse pinches) along shortened (or extended) single layers of relatively low effective viscosity (Talbot, 1999). In practice, most lithological boundaries are sufficiently widely spaced that the shear along them is so inconspicuous that it can be neglected in discussions of cleavage and strain refraction (e.g. Treagus and Sokoutis, 1992); this is because the boundary shears are overshadowed by the more spectacular deformation structures that develop along their intervening counterflow boundary.

The concept of counterflows along lithological boundaries and across uniform rocks is confined to the reference frame in Fig. 4(b) which shows the counterflow but not the absolute direction of flow. However, the material inhomogeneity responsible for counterflow along lithological contacts is visible within that reference frame, whereas the boundary condition responsible for counterflow in uniform rocks is not (as it is in Fig. 4a).

Just as shear failure in uniform rocks deforming as brittle solids can result in spontaneous new planar slip boundaries called fractures, so shear failure in uniform rocks deforming as pseudoplastic fluids can result in spontaneous new planar no-slip boundaries called counterflow boundaries. As we refer to individual faults, so can we refer to individual counterflow boundaries.

What have previously been described as individual symmetric shear zones in uniform rock (Fig. 5b) are here considered as coupled pairs of boundary shears. The geometries of these boundary shears can be identical but with mirror symmetry screwed about their mutual no-slip counterflow boundary so that their senses of shear remain constant. (Bundles of displacement curves are symmetric about a point on the counterflow boundary.) Such point symmetry derives from two bodies of rocks deforming as identical power law fluids having travelled in the same direction at bulk rates that differed by a factor of 2 because of boundary conditions not seen in Fig. 5(b). Boundary shears in uniform rocks flowing in the same direction at rates that differ by any factor other than 2 will be asymmetric by differing in maximum displacement but not necessarily width (Fig. 5c).

Not all boundary shears coupled across lithological boundaries distort to lobes or cusps (Fig. 5a). Similarly, most counterflow boundaries in uniform rocks remain straight in the frame of Fig. 4(b) whether or not they spin in a wider reference frame (Fig. 4a).

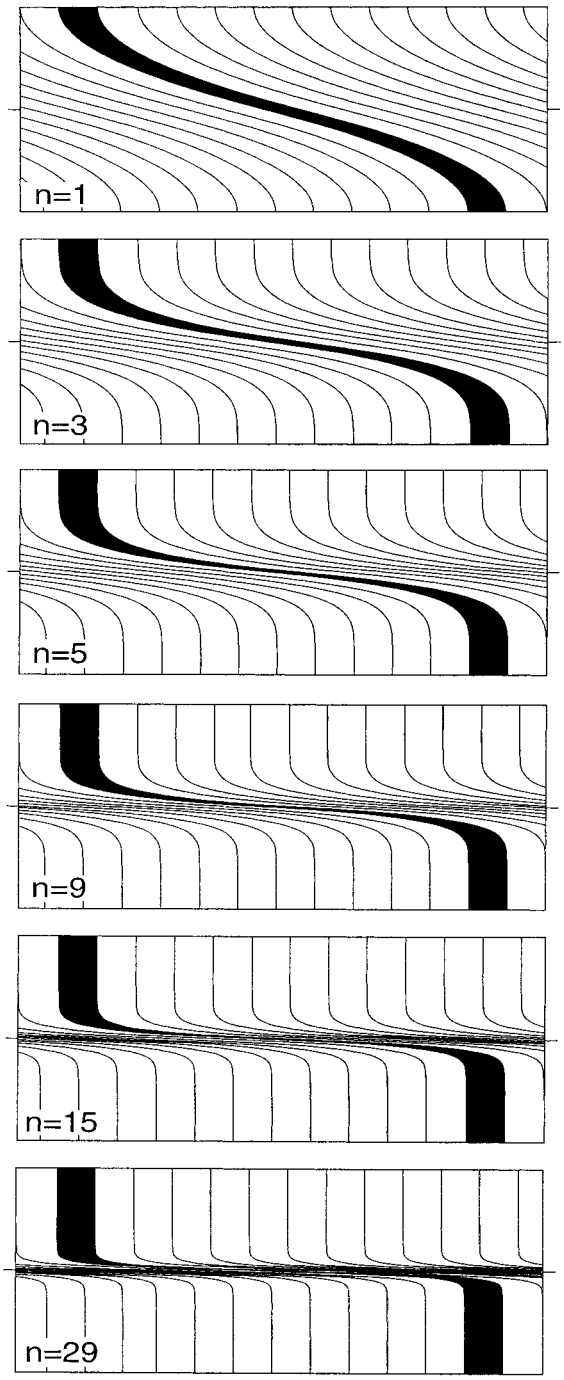

Fig. 6. Forward models of symmetric counterflow boundary shears in fluids with constant but different *n*-value (labelled). Counterflow boundaries are ticked at the end of each box.

4. Forward modelling of counterflow

Figure 6 shows profiles of forward physical models of symmetric coupled counterflow boundary shears in uniform rocks deforming as pseudoplastic fluids with the stress sensitivity of the strain rate (given by n) increasing in arbitrary steps in successive boxes downward. As in all previous figures, these boundary shears

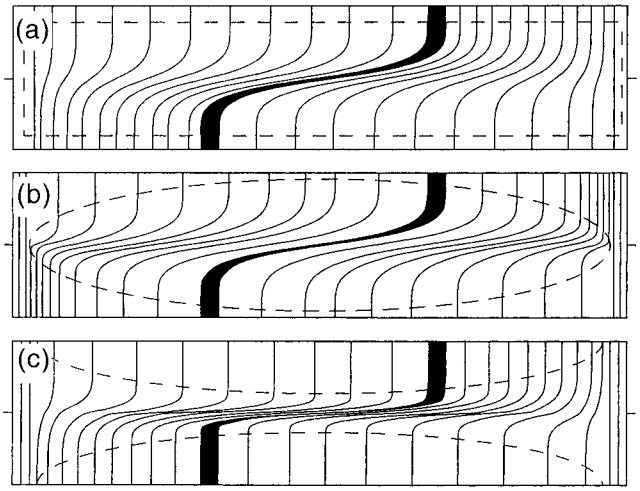

Fig. 7. As displacement accumulates, boundary shears in a pseudoplastic with $n = 3$ (with dashed margins) of (a) Type III maintain constant width, (b) Type I widen between converging ends and (c) Type II narrow between diverging ends.

were modelled graphically using repetitions of one or other of the curves in Fig. 2 which is based on Eq. (5). Contours of cumulative displacement and strain (not shown) are parallel (combed, or raked, cf. Lisle, 1992) in each block because the flows in both adjoining streams are (or were) homogeneous. Blackened stripes across each block emphasise that displacements are identical across each counterflow boundary (Fig. 6). The coupled boundary shears narrow and the strain gradients steepen systematically as the shear increasingly localises through the geometric and quantified mechanical spectrum. Boundary shear widths in each box of Fig. 6 remain constant, not just because displacements parallel the counterflow boundaries, but because n was also constant along their lengths.

4.1. Coupled boundary shears in pseudoplastic fluids with constant n

Whether natural coupled boundary shears change in width with time is not a simple matter (e.g. Means, 1984, 1995). However, spatial variations in width are most likely at their ends. Consider two adjoining streams of a uniform rock that begin to differ in velocity at one end of a counterflow boundary and resume equal velocities at the other end. The ends of such counterflow boundaries cannot involve simple shear alone because flow must accelerate on one side at one end and slow on the other side at the other end while maintaining material continuity (Fig. 7). Where markers at a high angle to the counterflow boundary change in spacing, other markers, *parallel* to the counterflow boundary (not shown), must change in length. Because of this direct linkage between changes in velocity and geometry, spatial changes in width at the

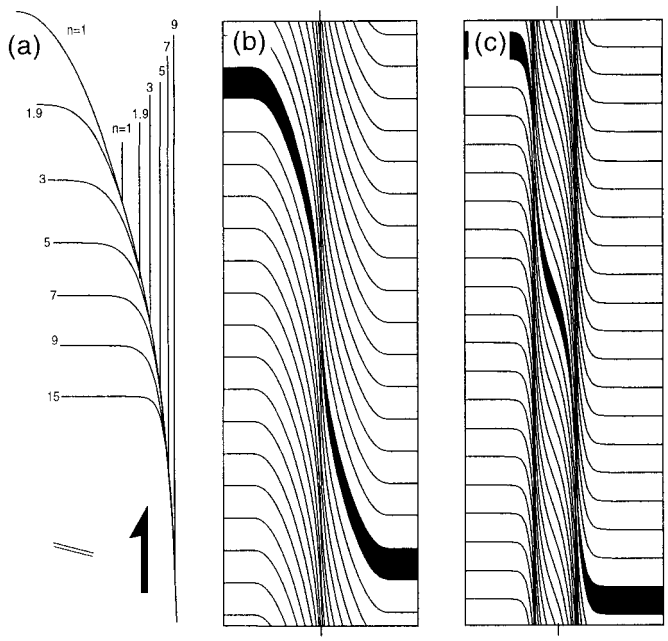

Fig. 8. (a) Displacement profiles across boundary shears in which n was rising with time can only be smooth where they pass one to another tangentially inward to the counterflow boundary. (b) Repetitions of part of this unique tangential curve model a counterflow boundary in which n increased from $n = 1$ to $n = 9$ with time. (c) Decreasing n-values in time leads to compound boundary shears with complex displacement profiles (here $n = 15$ to $n = 1$).

ends of countershears can be taken as proxies for changes of width in time, and spatial gradients along the stream lines as proxies for gradients in time.

If the counterflow is perpendicular to initially parallel straight marker lines, the relative acceleration and slowing at one end must match the relative slowing and acceleration at the other end (Fig. 7). The end geometries need only match (with screwed mirror symmetry) if the counterflow boundary has remained straight across straight marker lines.

The maximum displacement shown in Fig. 2 is entirely arbitrary. Changing the maximum displacement preserves the essential differences in displacement gradients along boundary shears with constant n-value so long as Eq. (5) is satisfied. The ends of coupled boundary shears in rocks with constant n-value can therefore be modelled by systematically changing the displacement and corresponding width in Eq. (5) while keeping n constant (Fig. 7). The shear strain gradients and marginal displacements decrease systematically on one side as they increase on the other; the reverse happens at the other end. It is therefore possible to model counterflow boundaries in which the width of both boundary shears remain constant (Fig. 7a), widen (Fig. 7b) or narrow (Fig. 7c) in space (and therefore past time) even though their ends cannot involve simple shear of constant volume in rocks of constant n. The changes in spacing between markers initially perpendicular to the counterflow boundary near its ends are idealised in Fig. 7 and may involve strain gradients that are unnaturally steep. Nevertheless, they illustrate the concept that the margins of counterflow boundaries can remain constant, or either widen or narrow in space and time. Means (1984) labelled ductile shears that widen with time as Type I zones and those that narrow with time as Type II; Fig. 7 illustrates that there may also be Type III that maintain constant width with time.

4.2. Coupled boundary shears in power law fluids with variable n

Careful inspection of the curves in Fig. 2 reveals that there is only a limited range where separate curves for velocity or displacement in Fig. 2 can pass smoothly (tangentially) from one to another (Fig. 8a). This suggests that displacement curves can increase smoothly and continuously inward toward counterflow boundaries in pseudoplastics with a limited range of n-values, within $n = 1$ to ≈ 15, (symmetrically in Fig. 8b). Such increasing localisation of deformation on the same counterflow boundary is likely in Type II ductile shears that narrow as n increases with time.

There are no equivalent smooth displacement curves for n-values decreasing inward toward the counterflow boundary over a significant range of n-values. Figure 8(c) is one of the smoothest curves I have managed empirically. Shear zones in which n has decreased during counterflow are likely to widen as Type I zones. The probable results are compound shear zones (Grocott and Watterson, 1980) characterised by irregular strain gradients and displacement profiles that do not fit the curves in either Figs. 2–8(a) (Fig. 8c). Possible natural examples have been illustrated by Mitra (1978, plate 1) and Segall and Simpson (1986, figs. 1 and 7).

5. Comparison with natural shear zones

Forward models of counterflow boundaries based on changing the n-value in Eq. (5) or Fig. 2 (see also Figs. 5–8) appear to successfully simulate the shear spectrum (as represented in Fig. 1). But is this approach relevant to rocks and does it have physical meaning?

To answer these questions, the displacement curves in Fig. 2 (from Eq. 5) will be compared with those in natural shear zones. The first step in such comparison is to identify on an appropriate outcrop, photograph, map or natural scale profile, etc., profiles that are close to parallel with the displacement directions along natural counterflow boundaries. The next is to mark on such a profile the apparent outer margins of

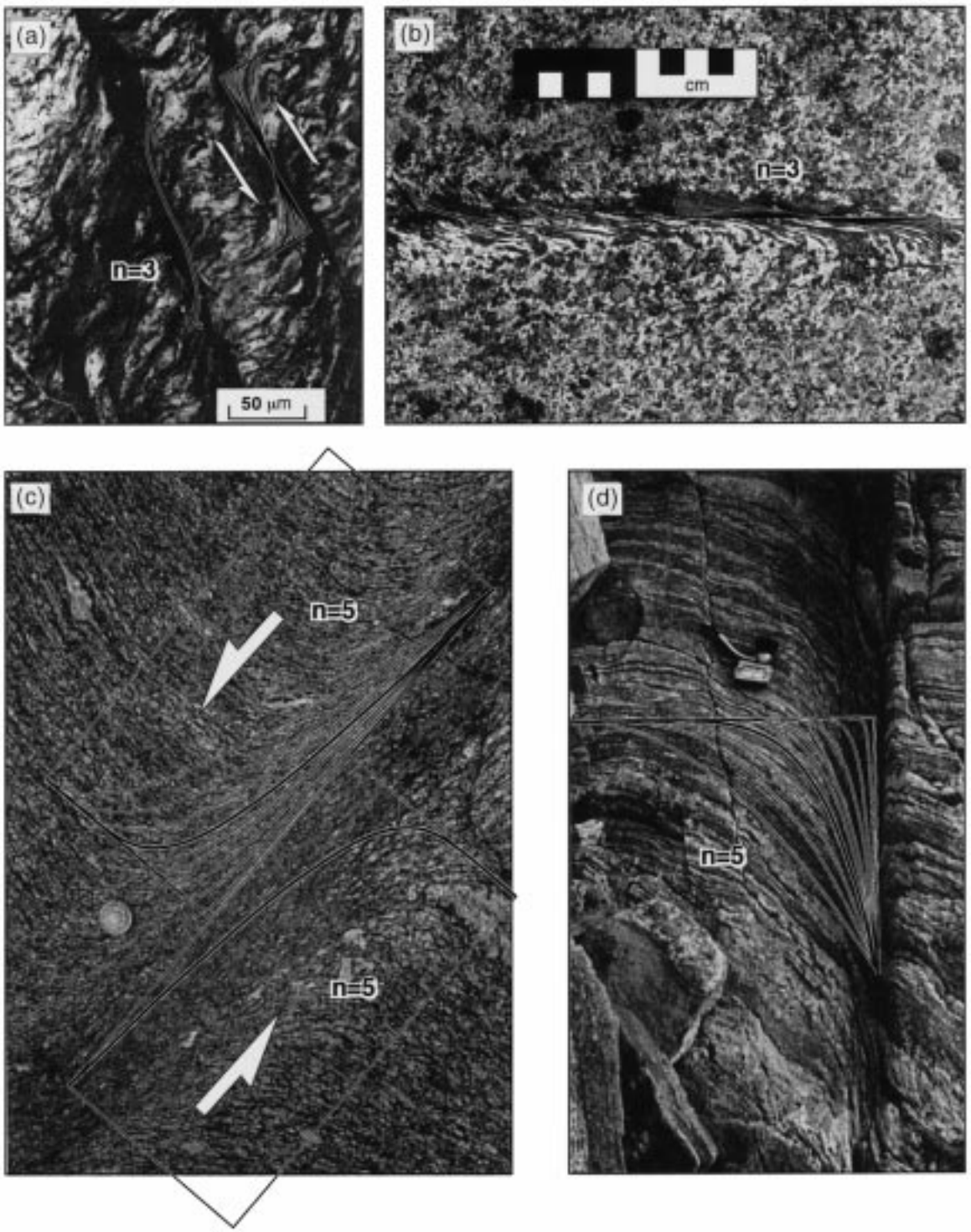

Fig. 9. Suitably scaled and distorted where necessary, one or other of the curves on Figs. 2 or 8(a) match a surprisingly high proportion of geological shears on a variety of scales (see text). (a) Crenulation cleavage in a slaty siltstone from the Moselelmunde (from Weijermars, 1986, fig. 4c). (b) A new foliation along a counterflow boundary in an almost isotropic gabbro at Vochalambina, Kola peninsula. (c) An older foliation distorted in granitoid gneisses at Cristallina, Swiss Alps (from Ramsay and Huber, 1983, fig. 3.18). (d) An asymmetric Nagssuqtoqidian counterflow boundary in Archaean migmatites near Holsteinsborg, W Greenland.

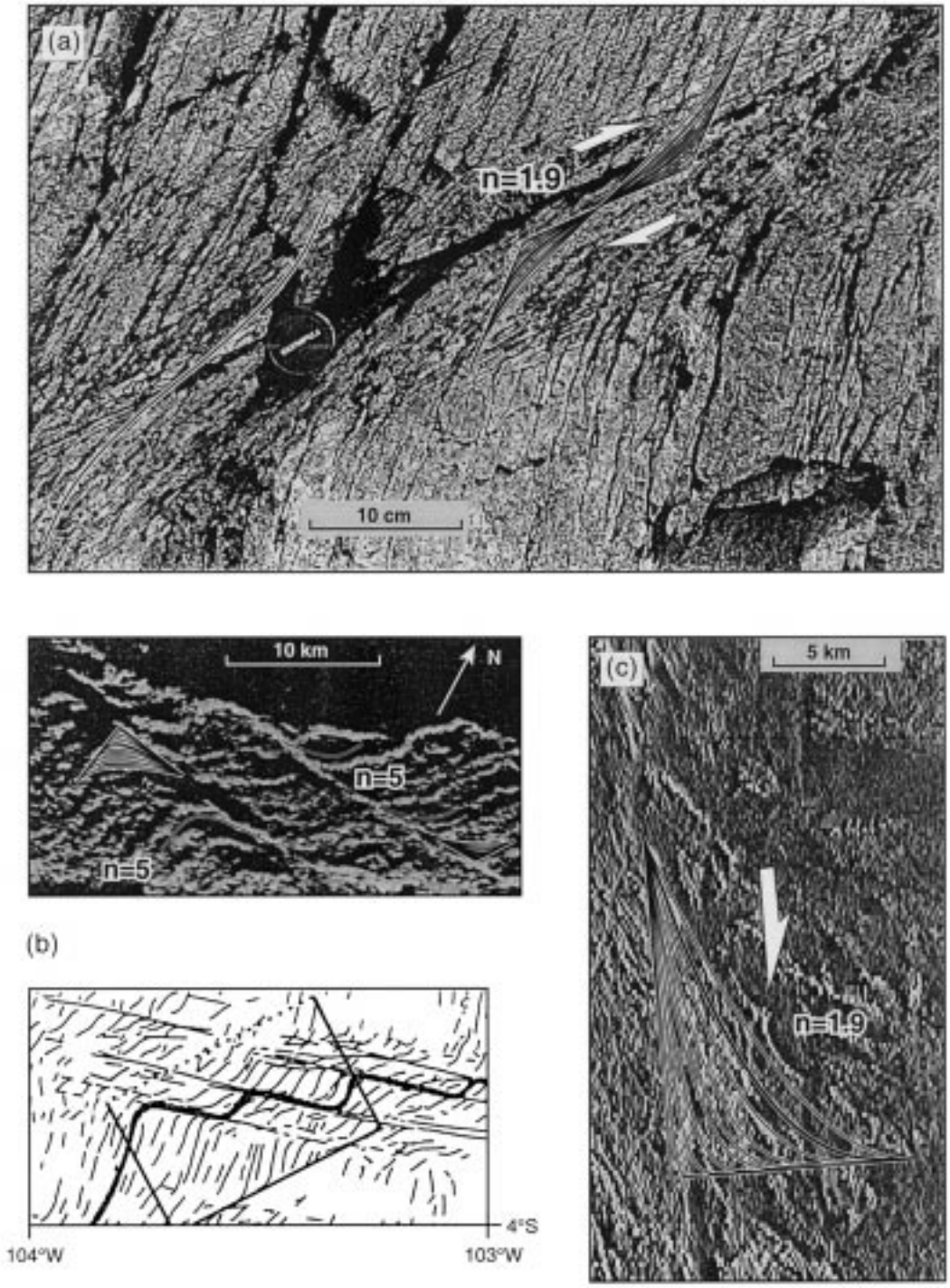

Fig. 10. (a) Late Hercynian symmetric counterflow boundary in sandstones at Roces Point near Cork, Ireland (from Trayner and Cooper, 1984). (b) Upper map: GLORIA image of part of the East Pacific rise (from Searle, 1983) located in lower map. (c) Aeromagnetic relief anomaly map of part of central Sweden. North is up the page in (b and c).

the boundary shears (where markers first depart from regional patterns) and the intervening counterflow boundary (which lies along the plane of greatest shear and zero relative displacement of strain markers). The non-dimensional curves of Figs. 2 or 8(a) are then scaled to the widths of each natural boundary shear and overlain on the profile to seek a fit. If the markers were not initially perpendicular to the counterflow boundary, or the displacement not twice the width of the boundary shear (as in Fig. 2), fits can be sought by applying Eq. (5) to markers with appropriate initial orientations and displacement, or

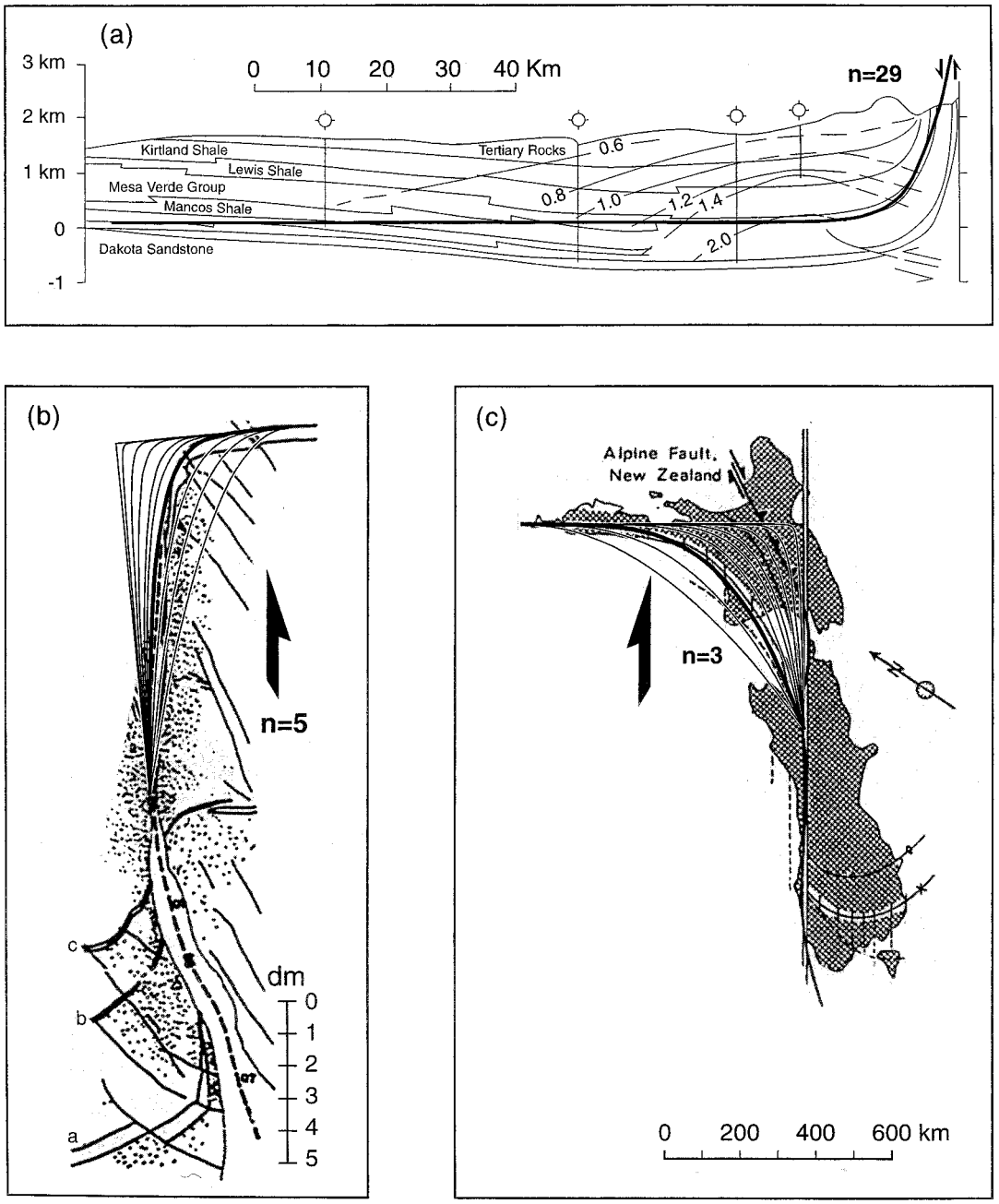

Fig. 11. (a) SW–NE profile across where the San Juan Basin abuts against the San Juan volcanic uplift in Colorado (from Law, 1992). (b) Aplites a, b and c distorted along a shear zone nucleated on a quartz vein (clear) in a granodiorite (dotted), Sierra Nevada, California (from Segall and Simpson, 1986, fig. 3). (c) The Alpine fault in New Zealand (from Weijermars, 1987, fig. 10).

by graphically distorting one or both the appropriate axes of Figs. 2 or 8(a) (natural examples are shown in Figs. 9–12).

A transparent montage of photocopies of Figs. 2 and 8(a) on a range of scales has been used in the field and literature (cited later) with considerable success to seek parts of boundary shears with appropriate markers and displacements. Figs. 9–12 illustrate analyses of counterflow boundaries in a wide variety of rock types, tectonic environments and types of image over a large range of scales. Every image analysed is assumed to be close to perpendicular to the counterflow boundary and parallel to past displacement trajectories along it. The examples of natural counterflow boundaries shown in Figs. 9 and 10 are arranged to fit the pages but will be discussed in general order of increasing scale and complexity.

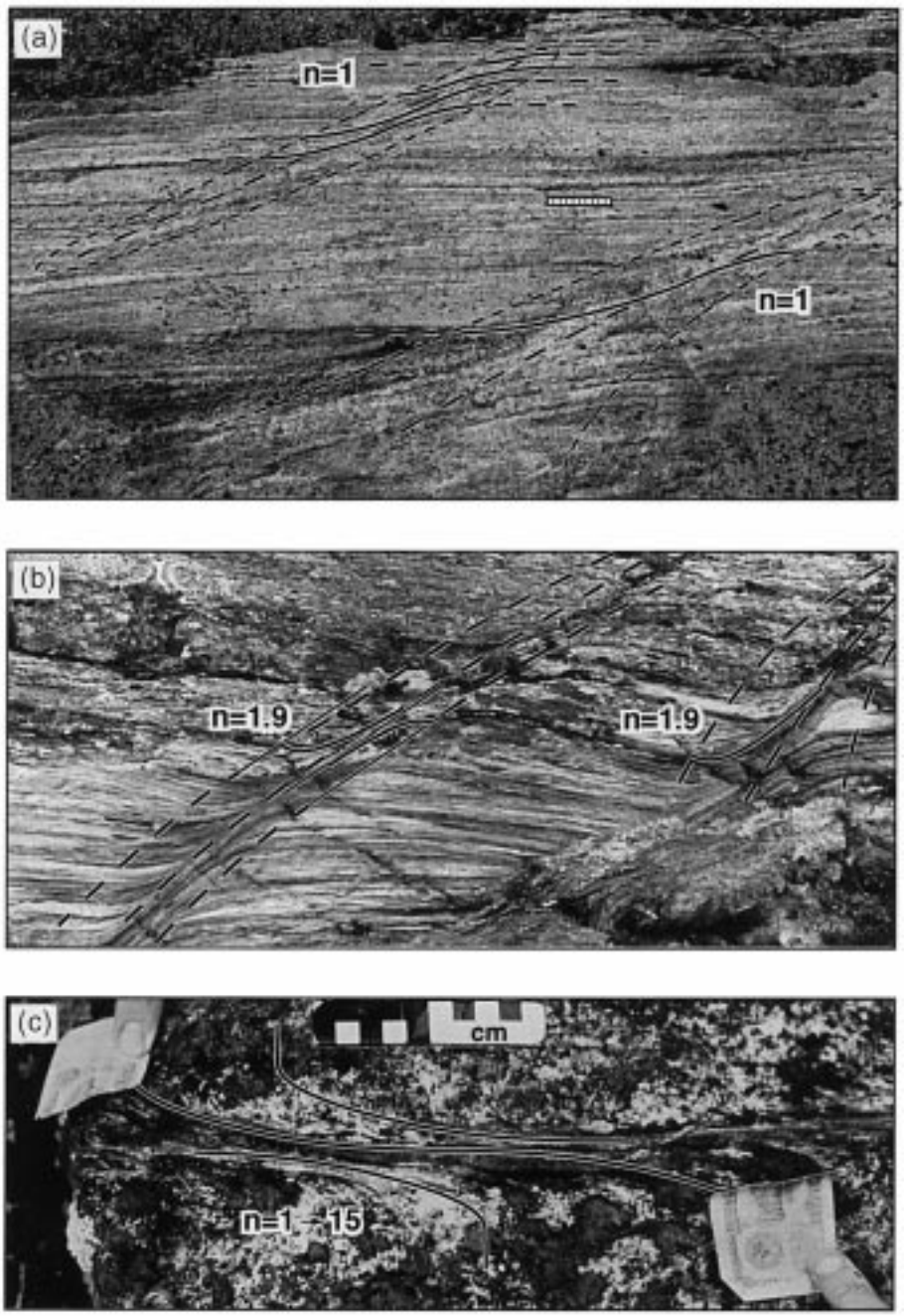

Fig. 12. (a) Counterflow boundaries (long dashes) with margins and ends (short dashes) in tonalitic Archaean gneisses, Kola peninsula, Russia. (b) Ultramafic rocks along the contact between the Seve and Koli nappes near Handöl, Scandinavian Caledonides (from Bergman and Sjöström, 1997, fig 5c). (c) Another counterflow boundary in the same gabbro at Vochalambina, Russia as illustrated in Fig. 9(b).

5.1. Results

Fig. 9(a) is a microphotograph of a crenulation cleavage distorting the first foliation in a slaty siltstone in the Moselelmunde of Germany (from Weijermars, 1986, fig. 4C). Fig. 2 has been repeated with screwed mirror symmetry about a single mutual no-slip counterflow boundary and shrunk and rotated to seek a geometric fit with the curvature of the crenulated foliation (right hand side of Fig. 9a). Only the (thickened) curves for $n = 3$ fit the curvature of the foliation clearly over most of the microphotograph. Two back-to-back $n = 3$ curves have been repeated alone to emphasise the generality of this fit (middle of Fig. 9a). Whatever deformations (volume changes, zone parallel extension, etc.) and whatever deformation mechanisms (crystal plasticity or solution, etc.) were involved, there is an empirical fit between this crenulation and a particular theoretical displacement gradient in boundary shears along unequally spaced counterflow boundaries.

Fig. 9(c) (from Ramsay and Huber, 1983, fig. 3.18) shows a counterflow boundary distorting an old foliation over widths of decimetres in granitoid gneisses at Cristallina in the Swiss Alps. Two superimposed back-to-back versions of Fig. 2 (necessarily offset) show that only the $n = 5$ curves fit the displacement gradients in two coupled boundary shears that are almost symmetrical in width and displacement. This counterflow boundary is thus attributed to adjoining masses of identical rock having flowed with constant $n = 5$ at velocities that differed on either side of the shared counterflow boundary by a factor close to 2 in a reference frame larger than shown.

The foliations distorted in Figs. 9(a) and (c) predated counterflow. The foliation in Fig. 9(b) was generated by the counterflow (cf. Fig. 3). Fig. 9(b) is a photograph by the author of part of a counterflow boundary a few metres long with a width of centimetres in the almost isotropic core of a $200\times >$ 500 m pod of gabbro exposed in Lopian supracrustal rocks (2.8–2.7 Ga) inside a greenstone belt within 300 m of the Bellomorian (3.15–2.9 Ga) granulite–gneiss terrain at Vochalambina in the Kola peninsula of Russia (Alekseev et al., 1993). This counterflow boundary probably developed in amphibolite metamorphic facies during the 2.5–1.8 Ga Karelian orogeny. The same doubled and partial versions of Fig. 2 as used in Fig. 9(a) have been rotated, scaled and superimposed to fit the new shear foliation. The unambiguous fit of the $n = 3$ displacement curve to the curvature of the foliation along two symmetrical boundary shears coupled across the counterflow boundary suggests that shear occurred with constant $n = 3$.

Fig. 9(d) shows another decimetre-scale counterflow boundary, one of Nagsuggtoqidian age distorting an older (Archaean) migmatite near Holsteinsborg in west Greenland. This differs from previous examples in that the sheared rock mass consists of multiple layers of different composition (and that the photograph is complicated by relief). Equation (5) and Fig. 2 refer to uniform materials but, on the basis that thin multilayers might exhibit a single bulk shear gradient, the maximum displacement on Fig. 2 was scaled to seek a fit for part of one boundary shear (Fig. 9d). The displacement gradient of the migmatitic layering was found empirically to fit only the $n = 5$ curve despite any strain activity of the layers. However, that this fit is only local, implies that strains along this boundary shear were not homogeneous (see later).

Fig. 10(a) (from Trayner and Cooper, 1984, fig. 3) illustrates the localised distortion of a crude cleavage developed axial planar to the Church Bay Anticline of Hercynian age in its northern limb at Roces Point near Cork in Ireland. Contours of displacement and shear strain parallel bedding and can be attributed to symmetric counterflow between two sandstones late in the folding. The width axes of the curves in Fig. 2 have been rotated by 46°, and the displacement scaled to match the distortion of the cleavage (Fig. 10a). The fit of the $n = 1.9$ displacement curve to both boundary shears (each about 1 dm wide) is inferred to constrain the constant stress sensitivity of the strain rate when the sandstones sheared during Hercynian folding.

The natural boundary shears analysed above have widths of decimetres or less, those shown in the two maps of Fig. 10(b) are considerably larger. The lower map locates the upper map which is an image produced by the long-range sidescan sonar GLORIA. This shows sigmoidal displacement patterns along the Quebrada Fracture zone (3.5°S) in the fast-spreading East Pacific Rise (from Searle, 1983). Narrow linear reflections are probably from fault scarps, broader reflections from linear volcanic ridges or the backs of tilted fault blocks. Searle interpreted this image in terms of four rapidly slipping transform faults offsetting closely spaced scarps of normal faults formed near the spreading axes (heavy line in lower map). "Such curvature is found universally near fracture zones although the degree of curvature and its spatial extent may vary somewhat" (Searle, 1983, p. 608). Suitably scaled, rotated and distorted versions of curves from Fig. 2 are superimposed to support the alternative interpretation offered here: that the image shows coupled counterflow boundary shears with displacement gradients that fit the $n = 5$ curve at least locally (see later). This alternative interpretation ignores any counterslip (additional to the counterflow) but raises the possibility that ocean floor near transforms is not always brittle but can deform as a pseudoplastic fluid at some stage (see later).

Fig. 10(c) is an aeromagnetic relief anomaly map (by courtesy of the Swedish Geological Survey) of part of the Storsjön–Edsbyn deformation zone in granitoid basement of Sveccofennian age (1.85–1.70 Ga) in central Sweden (Bergman and Sjöström, 1994). As in Fig. 9(d), the markers distorted in this strike-flow boundary shear vary in lithology but here on scales of tens of kilometres. Like many shear zones exposed in old basement rocks, this example reactivated several times in different P–T conditions both below and above the ductile–brittle transition. The nearly N–S-trending magnetic lows in Fig. 10(c) are later faults (< 1.6 Ga) but do not affect the unique local match of $n \approx 1.9$ curves from Fig. 2. The aeromagnetic relief anomalies are attributed to the preservation of a pattern imposed when bulk shear occurred at upper amphibolite facies.

Fig. 11(c) shows a map of the Alpine fault in New Zealand (from Weijermars, 1987, fig. 10), a continental shear on an even larger scale than that in Fig. 10(c). Only the $n = 3$ curve of a suitably distorted version of Fig. 2 fits the curvature of a marker band outside and inside the western boundary shear for hundreds of

kilometres. A 'drag fold' along the Alpine fault can be interpreted as having the displacement pattern of an asymmetric counterflow boundary on the scale of the continental lithosphere that sheared with $n = 3$. Like the other examples on smaller scales (Figs. 10b and c), counterslip assumed to post-date the counterflow is ignored here. The surficial rocks are obviously brittle and fractured but the pattern visible on the scale of Fig. 11(c) is either inherited from when the surface rocks were ductile and shearing with $n = 3$ at depth, or transmitted from such rocks through their brittle carapace. In either case it is the n-value effective during ductile shear that has been measured. All the natural examples illustrated here preserve the effects of particular episodes of ductile shear even though they are exposed in rocks that are now presumably brittle.

The contact between the San Juan Basin in New Mexico and the San Juan volcanic uplift in Colorado is currently interpreted as a normal fault. However, the thick curve superimposed on the SW–NE profile (Fig. 11a, after Law, 1992) is the curve for $n \approx 29$ found empirically to fit the boundary between the Mancos shale and the Mesaverde sandstones after scaling Fig. 2 to match the strata (shown with a vertical scale 11.3 times the horizontal scale). This fit raises the possibility that these Upper Cretaceous to Eocene shales and sandstones underwent normal dip-flow in a boundary shear with a width of tens of kilometres against the flanks of the San Juan uplift in Laramide (early Tertiary) times. The age of contours of thermal maturity (vitrinite reflectance, labelled 0.6–2.0) relative to the shearing is not clear. A reviewer of an earlier version of this work suggested that another exponential law would probably provide a better rheological approximation to the sediments represented in Fig. 11(a). However, the best fit possible for the other exponential curve treated to the same scaling as the $n \approx 29$ curve is not shown as it is nowhere near as good as the curve shown for pseudoplasticity and would obscure the profile. Similar fits for that other exponential curve have been attempted for all the natural examples shown here and the pseudoplastic fits are significantly better in every case.

Fig. 11(b) (from Segall and Simpson, 1986, fig. 3) illustrates coupled boundary shears decimetres wide in a granodiorite of the Sierra Nevada of California. Segall and Simpson (1986) considered that the ductile shear nucleated on a dilatant fracture filled by quartz before minor offsets occurred along fractures. Superimposing the curves of Fig. 2 on aplite (a) in the right hand boundary shear suggests that $n \approx 5$ and was constant during the ductile shear.

Fig. 12(a) shows the complete lengths of two parallel counterflow boundaries in tonalitic gneisses of Archaean age in the Shirokaya area on the Kola peninsula of Russia. Some of the distorted markers are overlain by heavy lines after the curves in Fig. 2 were distorted to match their curvature. This match was entirely successful for the $n = 1$ curve but no others (Fig. 12a). Remembering that the ends of counterflow boundaries cannot involve simple shear alone, it is intriguing to note that the lower ends of one counterflow boundary converge whereas the others diverge; that to the right may have narrowed in time (cf. Fig. 7b) whereas that to the right, which has a neosome segregation vein along most of its length, may have widened with time (cf. Fig. 7c). Both the upper ends can be interpreted as having maintained constant width as these migmatites sheared as Newtonian fluids.

Fig. 12(b) is a photograph of foliated ultramafic rocks shredded among ophiolites along the contact between the Seve and Köli nappes near Handöl in the Scandinavian Caledonides (from Bergman and Sjöström, 1997, fig. 5B). Two asymmetric extensional counterflow boundaries affected the early foliation over widths of decimetres. Scaling, distortion and rotation of Fig. 2 to seek fits between the curvature of the foliation and the various n-curves (not shown) found that the $n \approx 1.9$ curve generally matches along each boundary shear suggesting that these rocks deformed with a constant stress sensitivity of the strain rate near 1.9 in late Caledonian times. The two marker foliae overlain by $n \approx 1.9$ curves to the left in Fig. 12(b) are on either side of a small change in composition across which the superposed foliation is slightly oblique. On a close-up photograph (not shown) the two foliae refract across the counterflow boundary and have angles of 34° and 45° from the perpendicular to the counterflow boundary beyond the margins of the boundary shears. Applying eq. (4) of Treagus and Sokoutis (1992) implies a ratio of effective viscosities of ≈ 1.3 across the lithological boundary during shear. Such details probably account for the variable width of the boundary shears on either side of the counterflow boundary to the left. Thus both counterflowing bodies deformed with $n \approx 1.9$ but the displacement was greater in the boundary shear deforming with lower effective viscosity.

Fig. 12(c) is the only counterflow boundary known to the author across which markers (a new foliation) fit a suitably scaled version of the curve in which n-values increase smoothly toward the counterflow boundary (Fig. 8a). The curvature of the foliation in the centimetre-scale grains of the marginal gabbro indicates $n \approx 1$ and n appears to have systematically increased inward so that the fine-grained epidotic mylonite along the counterflow boundary itself deformed with $n \approx 15$. This counterflow boundary is only a few tens of metres away from that illustrated in Fig. 9(b) in the same pod of gabbro in the Kola peninsula of Russia. These two counterflow boundaries are both symmetric and affect similar widths in the same

isotropic gabbro. However, they are not parallel and while the counterflow in Fig. 9(b) clearly fits a constant $n = 3$ displacement curve (Fig. 2), that in Fig. 12(c) just as clearly fits the tangential curve for n increasing from 1 to 15 (Fig. 8b). The obvious interpretation is that the counterflow boundary with an inward decrease in grain size but not mineralogy (Fig. 9b) was short-lived and developed while conditions changed little. In contrast, the counterflow boundary in which marginal amphibolite gives way inward to greenschist facies minerals (Fig. 12c) was comparatively long-lived and the n-value rose as conditions changed during active shear. The coupled boundary shears in Fig. 12(c) probably narrowed with time as a Means type II shear zone.

6. Discussion

6.1. n-curves are robust

Suitably scaled or distorted, one or other of the theoretical curves in Figs. 2 8(a) fit the curvature of planar fabrics distorted along parts of natural boundary shears in a variety of rock types and environments on a wide range of scales (Figs. 9–12). The method introduced here therefore appears to be remarkably robust for limiting n-values of adjoining rock masses when they sheared. This is because the displacement profiles (Figs. 2–8a) remain distinctive whatever the width, maximum displacement and orientation of pre-existing passive markers. Furthermore, these curves remain distinctive through all combinations of simple and pure shears and/or volume changes that are smooth across the counterflow boundary and constant along it. It is possible to strain the individual $n = 1$–15 curves in Fig. 2 to resemble one another by applying either particular simple shears along the width axis, or particular pure shears along the line joining where the curves meet the displacement and width axes. As neither of these special types of strain are likely to affect natural counterflow boundaries, the curves in Figs. 2 or 8(a) remain recognisable through most likely natural deformations. The geometric fits demonstrated in Figs. 9–12 therefore measure the stress sensitivity of the strain rate of the rocks when they sheared whatever other deformations occurred. The constraints of the measured shear being only simple and isochoric may be dropped from the initial assumptions.

Many of the fits illustrated on Figs. 9–12 are only local. The markers are local in Fig. 11 and the fits are local in Figs. 9(d), 10(b) and (c) and 12(a). The remaining initial assumptions, of steady continuous homogeneous deformation, are inappropriate for these cases. Deformation was clearly not homogeneous along these zones and it is unlikely that they were either steady or continuous.

6.2. Effective steadiness and continuity of accumulated shear

The generality of the empirical fits between theoretical finite displacement curves for steady flow of pseudoplastic fluids (Fig. 2) and the curvature of natural markers *along* the natural counterflow boundaries in Figs. 9(a–c), 10(a), 12(b) and (c) has significant implications. Whether or not the flows occurred in irregular episodes of different length because stresses varied with time, the flows responsible for these cases *appear* to have accumulated steadily and continuously; they can therefore be treated as such *on the scale of the analyses*. This is attributed to the analyses being on scales many orders of magnitude larger than the scales on which the deformation mechanisms occurred.

6.3. General deformations

Displacement curves along the main body of natural counterflow boundaries show a conspicuous tendency to be described by Eq. (5). However, as already emphasised, departures from homogeneous strains are inevitable near the ends of counterflow boundaries as a result of flow maintaining continuity during change in velocity (Fig. 12a). The symptoms of such complications are either curvature of the counterflow boundary itself, and/or contours of displacement or strain that narrow or widen in planar sections, often asymmetrically. Contours of displacement and strain are likely to diverge toward boundary conditions that retard flow and constrict the fluid (McCoss, 1986). They are likely to converge away from boundary conditions that accelerate flow and flatten the fluid (McCoss, 1986). The shapes of contours of displacement or strain thus provide a simple indication of how the style of strain varies along counterflow boundaries.

6.4. Alternatives to power law shears?

It is still significant if, after any combination of scaling, rotation or distortion, none of the theoretical curves on Figs. 2 or 8(a) fit the curvature of markers sheared along natural boundary shears. Perhaps the counterflow boundary or displacement trajectories were curved or oblique to the profile so that shear was not homogeneous parallel to the margins. Perhaps the markers were strain active (Ramsay and Huber, 1983)

and some counterflows have certainly been subsequently distorted (unpublished). There may also be (large and fast?) boundary shears in which displacement gradients fit models other than power law.

6.5. Variations in n

The stress histories of old basement rocks can be expected to have changed as their boundary conditions changed in response to the opening and closing of surrounding oceans (e.g. Munier and Talbot, 1993). While the rocks were still sufficiently deep and warm to be ductile, shear can be expected to increasingly localise in new counterflow boundaries with different orientations as the n-value decreased as P–T conditions changed. Nevertheless, n-values can be expected to be constant in individual examples of successive generations of new counterflow boundaries—as was found for most of the natural examples analysed here.

By contrast, plutons (e.g. Gapais, 1989) might cool sufficiently rapidly that their n-values could increase without significant changes in boundary conditions. If so, strain can be expected to increasingly localise to the same continuously active counterflow boundary—as was found in Fig. 12(c) here.

6.6. The physical meaning of n

While discussing the effects that control the rates at which rocks strain, Means (1990, pp. 968–969) wrote "At lower strain rates, the temperature weakening effect dominates the pressure strengthening effect and so, ... in general, increases in confining pressure or temperature promote ductility ... . The relation of temperature to steady state flow stress and strain rate is commonly found to fit a flow law of the form of":

$$\dot{e} = A\sigma^n \exp(-Q/RT) \quad (6)$$

which is more explicit about the constant in Eq. (1c) (e.g. Nye, 1957).

In Eq. (6), A is a constant characteristic of the system considered, Q is the activation energy of a steady process, R is the gas constant, T the absolute temperature, and n is the rheological parameter that expresses the stress sensitivity of the strain rate.

In mineralogy, the system considered in Eq. (6) might be a single mineral phase and Q might refer to specific sub-microscopic deformation mechanisms (e.g. Birger, 1998). In petrology and rock mechanics, the system might be a single rock type and Q might refer to steady creeping flow; here the systems considered have been counterflow boundaries in individual rock types or compound rock units and Q is that of the counterflow.

Notice that the various parameters on the right hand side of Eq. (6) could vary independently (although A is related to T) so that, e.g. n can be independent of T. In polymers used as analogues of rocks in dynamically scaled deformation models, n can remain constant over a range of temperatures (Hailermariam and Mulugeta, 1998). In the rock mechanics literature, n is expected to vary with grain size so that $n = 1$ for ultra-fine rocks and $n = 2.5$–4.5 for coarser-grained rocks (e.g. Ranalli, 1995). This appears to be the reverse of what is seen in Fig. 12(c) where other variables may have been more significant.

The analyses of Figs. 9–12 found that crystalline metamorphic rocks appear to shear with $n = 1$ when melting (Fig. 12a), with $n = 1.9$–3 at amphibolite facies (Figs. 9b, 10c and 12b) and $n \approx 5$ in metamorphic facies of lower grade (Figs. 9c and d and 11b). The slaty siltstone sheared with $n = 3$ and the sandstones with 1.9 at low metamorphic grade (Figs. 9a and 11a) and unmetamorphosed sediments can be interpreted as having sheared with $n \approx 2.9$ (Fig. 11a). In general, the stress sensitivity of the strain rate of rocks and rock masses appears to increase with decrease in both P and T.

7. Summary

Empirical fits exist between theoretical displacement curves for steady flows of pseudoplastic fluids along boundary shears and the displacement gradients in natural deformation zones (and 'drag folds' along faults). These fits are, in effect, simple measurements of the stress sensitivity of the strain rate of specific rock types deformed over particular time intervals in conditions of P–T–$\dot{\varepsilon}$-fluid that can be constrained by other methods. The relative notions of penetrative strains and competence in ductile rocks can now be replaced by routine assignment of n-values.

The concept of counterflow boundaries potentially allows resolution of many problems previously associated with shear zones. Thus constraining absolute ages of pre-, syn-, and/or post-shear markers would also limit the relative strain rates for rock masses for which the n-value can be measured. Whether strains that take years or less in particular rocks deformed in laboratories and millions of years in nature occur by different processes (Means, 1990) can now be checked. Structural and tectonic modellers currently use small scale laboratory measurements but in future could use field readings of n-values of particular rocks on appropriate scales in relevant P–T environments.

Acknowledgements

Jonas Helborn and Alexai Poliakov are thanked for

programming displacement profiles that ended as Figs. 1–6. The scepticism of Joseph Hull, Ruud Weijermars, Roberto Weinberg, Kieran Mulchrone, Yuri Podladchikov, Dazhi Jiang, Sue Treagus, Win Means, Surendra Saxena and Bertram Schott helped me refine some of these ideas. The surviving mistakes are all mine. Christina Wernström is thanked for helping with Figs. 9–12 and Kajsa Hult of the Swedish Geological Survey, for supplying the map used in Fig. 10(b).

This work developed out of field observations in W. Greenland in 1967, Saskatchewan in 1968, and more recent observations in Sweden funded by NFR, the Swedish Natural Science Foundation and SKB, the company responsible for managing Sweden's nuclear fuel and waste.

References

Alekseev, V., 1993. Structural associations at different lithospheric levels of the Kola peninsula, the Baltic Shield. In: Unzog, W., Walbrecher, E., Brandmayr, M. (Eds.), Structures and Tectonics at Different Lithospheric Levels. Blackwell Scientific, Oxford.

Beach, A., 1985. Retrogressive metamorphic processes in shear zones with special reference to the Lewisian complex. Journal of Structural Geology 2, 257–263.

Bergman, S., Sjöström, H., 1994. The Storsjön–Edsbyn deformation zone, central Sweden. Research report to the Geological Survey of Sweden, Box 670, S-751 28 Uppsala, Sweden.

Bergman, S., Sjöström, H., 1997. Accretion and lateral extension in an orogenic wedge: evidence from a segment of the Seve–Köli terrane boundary, central Scandinavian Caledonides. Journal of Structural Geology 19, 1073–1091.

Birger, B.I., 1998. Rheological model of the Earth and a thermoconvective mechanism for sedimentary basin formation. Geophysical Journal International 134, 1–12.

Fletcher, R.C., 1974. Wavelength selection in the folding of a single layer with power law rheology. American Journal of Science 274, 1029–1043.

Gapais, D., 1989. Shear structures within deformed granites, mechanical and thermal indicators. Geology 17, 1144–1147.

Grocott, J., Watterson, J., 1980. Strain profile of a boundary within a large ductile shear zone. Journal of Structural Geology 2, 111–118.

Hailermariam, H., Mulugeta, G., 1998. Temperature-dependent rheologies of bouncing putties used as rock analogs. Tectonophysics 294, 131–141.

Harris, L.B., Cobbold, P.R., 1984. Development of conjugate shear bands during bulk simple shearing. Journal of Structural Geology 7, 37–44.

Harris, J., 1977. Rheology and Non-Newtonian Flow. Longman, London.

Heard, H.C., 1968. Steady-state flow in Yule marble at 500–800°C. American Geophysical Union Transactions 49, 312.

Jiang, D., White, J.C., 1995. Kinematics of rock flow and the interpretation of geological structures, with particular reference to shear zones. Journal of Structural Geology 17, 1249–1265.

Jiang, D., 1994. Vorticity determination, distribution, partitioning and the heterogeneity and non-steadiness of natural deformations. Journal of Structural Geology 16, 121–130.

Kameyama, M., Yuen, D.A., Fujimoto, H., 1997. The interaction of viscous heating with grain-size dependent rheology in the formation of localised slip zones. Geophysical Research Letters 24, 2523–2526.

Law, B.E., 1992. Thermal maturity patterns, San Juan Basin, Colorado and New Mexico. Geological Society of America Bulletin 104, 192–207.

Lisle, R.J., 1992. Constant bed-length folding: three dimensional geometric implications. Journal of Structural Geology 14, 431–435.

Lister, G.S., Williams, P.F., 1979. Fabric development in shear zones: theoretical controls and observed phenomena. Journal of Structural Geology 1, 283–297.

McCoss, A., 1986. Simple construction for deformation in transpression/transtension zones. Journal of Structural Geology 8, 715–718.

Means, W.D., 1984. Shear zones of Types I and II and their significance to reconstruction of rock history. Geological Society of America, Abstracts with Program 16, 50.

Means, W.D., 1990. Kinematics, stress, deformation and material behavior. Journal of Structural Geology 12, 953–971.

Means, W.D., 1995. Shear zones and rock history. Tectonophysics 247, 157–160.

Mitra, G., 1978. Ductile deformation zones and mylonites. American Journal of Science 278, 1057–1084.

Munier, R., Talbot, C.J., 1993. Segmentation, fragmentation and jostling in cratonic basement near Äspö, Southeast Sweden. Tectonics 12, 713–727.

Nye, J.F., 1957. The distribution of stress and velocity in glaciers and ice sheets. Proceeding of the Royal Society of London, Series A 239, 113–133.

Poirier, J.P., 1980. Shear localisation and shear instability in materials in the ductile field. Journal of Structural Geology 2, 135–142.

Ramsay, J.G., Graham, R.H., 1970. Strain variation in shear belts. Canadian Journal of Earth Sciences 7, 786–813.

Ramsay, J.G., Huber, M.I., 1983. The Techniques of Modern Structural Geology: Volume 1: Strain Analysis. Academic Press, London.

Ramsay, J.G., 1967. Folding and Fracturing of Rocks. McGraw-Hill, New York.

Ramsay, J.G., 1980. Shear zone geometries: a review. Journal of Structural Geology 2, 83–100.

Ranalli, G., 1995. Rheology of the Earth, 2nd ed. Chapman & Hall, London.

Searle, R.C., 1983. Multiple, closely spaced transform faults in fast-slipping fracture zones. Geology 11, 607–610.

Segall, P., Simpson, C., 1986. Nucleation of ductile shear zones on dilatant fractures. Geology 14, 56–59.

Simpson, C., De Paor, D.J., 1993. Strain and kinematic analysis in general shear zones. Journal of Structural Geology 15, 1–20.

Smith, R.B., 1977. Formation of folds, boudinage, and mullions in non-Newtonian materials. Geological Society of America Bulletin 88, 312–320.

Tackley, P.J., 1998. Self consistent generation of tectonic plates in three dimensional mantle convection. Earth and Planetary Science Letters 157, 9–22.

Talbot, C.J., 1999. Can field data constrain rock viscosities. Journal of Structural Geology 21, 949–957.

Trayner, P.M., Cooper, M.A., 1984. Cleavage geometry and the development of the Church Bay Anticline, Co. Cork, Ireland. Journal of Structural Geology 6, 83–87.

Treagus, S., Sokoutis, D., 1992. Laboratory modelling of strain variations across rheological boundaries. Journal of Structural Geology 14, 405–424.

Turcotte, D.I., Schubert, G., 1982. Geodynamics, Application of Continuum Physics to Geological Problems. Wiley, New York.

Weijermars, R., 1986. S1-cleavage fans in the Moselelmunde of the Rheinische. Geologische Rundschau 75, 323–332.

Weijermars, R., 1987. The construction of shear strain profiles across brittle–ductile shears. Annales Geophysicae 5B, 201–210.

Wilkinson, W.L., 1960. Non-Newtonian Fluids. Pergamon Press, Oxford.